We are IntechOpen,
the world's leading publisher of
Open Access books
Built by scientists, for scientists

4,800
Open access books available

122,000
International authors and editors

135M
Downloads

154
Countries delivered to

Our authors are among the

TOP 1%
most cited scientists

12.2%
Contributors from top 500 universities

CLARIVATE ANALYTICS
BOOK CITATION INDEX
INDEXED

WEB OF SCIENCE™

Selection of our books indexed in the Book Citation Index
in Web of Science™ Core Collection (BKCI)

Interested in publishing with us?
Contact book.department@intechopen.com

Characterization for Dynamic Recrystallization Kinetics Based on Stress-Strain Curves

Quan Guo-Zheng

Additional information is available at the end of the chapter

http://dx.doi.org/10.5772/54285

1. Introduction

Most metals and alloys have become increasingly important in a variety of applications. The most important of these properties are ease of high strength, relatively good ductility, and good corrosion resistance. One of the ways of acquiring the best combination of these properties is to select the microstructure, which in turn depends on thermo-mechanical history as well as on chemical composition [1]. An optimization of the thermo-mechanical process can be achieved through an understanding of the entire forming process and the metallurgical variables affecting the micro-structural features occurring during deformation operations carried out during deformation operations carried out at high temperatures. Most applications of these alloys are in the chemical process equipment, petrochemical, aerospace industry, and medical tools. The understanding of metals and alloys behavior at hot deformation condition has a great importance for designers of hot metal forming processes (hot rolling, forging and extrusion) because of its effective role on metal flow pattern, and the constitutive relationships are often used to describe the plastic flow properties of metals and alloys in a form that can be used in computer code to model the forging response of mechanical part members under the prevailing loading conditions [2].

During hot forming process alloy is liable to undergo work hardening (WH), dynamic recovery (DRV) and dynamic recrystallization (DRX), three metallurgical phenomena for controlling microstructure and mechanical properties [3]. The relay of softening mechanism from strain-hardening and dynamic recovery to DRX is the reason the term discontinuous has been earned. At a microstructural level DRX begins when strain hardening plus recovery can no longer store more immobile dislocations. When the critical strain is reached, on face centered cubic (fcc) metals of medium to low stacking fault energy, strain-hardening and dynamic recovery cease to be the principle mechanisms responsible of the stress-strain response, DRX accompanies

the process. However, DRX is not a phenomenon restricted to fcc metals, it has been described on ice, some minerals, and even high purity α–Fe (bcc metal) [4-6]. In the deformed material DRX would affect the crystallographic texture and thus, material anisotropy. For example, DRX would eliminate some crystal defects, such as part of dislocations resulting from work hardening, which will improve hot plasticity, refine microstructure, and reduce the deformation resistance [7]. High stacking fault energy (SFE) metals, such as aluminium alloys, alpha titanium alloys, and ferritic steels, undergo continuous dynamic recrystallization (CDRX) rather than discontinuous dynamic recrystallization (DDRX) during high temperature deformation. In particular, due to the high efficiency of dynamic recovery, new grains are not formed by a classical nucleation mechanism; the recrystallized microstructure develops instead by the progressive transformation of subgrains into new grains, within the deformed original grains. Dislocations produced by strain hardening accumulate progressively in low-angle (subgrain) boundaries (LABs), leading to the increase of their misorientation angle and the formation of high-angle (grain) boundaries (HABs), when a critical value of the misorientation angle is reached. The microstructure is thus intermediate between a subgrain and a grain structure: while grains and subgrains are entirely delimited by HABs and LABs, respectively, it will be referred to as an aggregate of crystallites, which are bounded partly by LABs and partly by HABs. On the contrary, low stacking fault energy (SFE) metals, such as magnesium alloys, austenitic steels, and beta titanium alloys, undergo discontinuous dynamic recrystallization (DDRX) rather than continuous dynamic recrystallization (CDRX) during high temperature deformation [8].

2. Description of softening flow behavior coupling with DRX

Hot working behavior of alloys is generally reflected on flow curves which are a direct consequence of microstructural changes: the generation of dislocations, work hardening, WH, the rearrangement of dislocations, their self-annihilation, and their absorption by grain boundaries, DRV, the nucleation and growth of new grains, DRX. The latter is one of the most important softening mechanisms at high temperatures. This is a characteristic of low and medium stacking fault energy, SFE, materials e.g., γ-iron, the austenitic stainless steels, and copper. The most significant changes in the structure-sensitive properties occur during the primary recrystallization stage. In this stage the deformed lattice is completely replaced by a new unstrained one by means of a nucleation and growth process, in which practically stress-free grains grow from nuclei formed in the deformed matrix. The orientation of the new grains differs considerably from that of the crystals they consume, so that the growth process must be regarded as incoherent, i.e. it takes place by the advance of large-angle boundaries separating the new crystals from the strained matrix [1].

DRX occurs during straining of metals at high temperature, characterized by a nucleation rate of low dislocation density grains and a posterior growth rate that can produce a homogeneous grain size when equilibrium is reached. The process of recrystallization may be pictured as follows. After deformation, polygonization of the bent lattice regions on a fine scale occurs and this results in the formation of several regions in the lattice where the strain energy is

lower than in the surrounding matrix; this is a necessary primary condition for nucleation. During this initial period when the angles between the sub-grains are small and less than one degree, the sub-grains form and grow quite rapidly. However, as the sub-grains grow to such a size that the angles between them become of the order of a few degrees, the growth of any given sub-grain at the expense of the others is very slow. Eventually one of the sub-grains will grow to such a size that the boundary mobility begins to increase with increasing angle. A large angle boundary, $\theta \approx 30\text{~}40°$, has a high mobility because of the large lattice irregularities or 'gaps' which exist in the boundary transition layer. The atoms on such a boundary can easily transfer their allegiance from one crystal to the other. This sub-grain is then able to grow at a much faster rate than the other sub-grains which surround it and so acts as the nucleus of a recrystallized grain. The further it grows, the greater will be the difference in orientation between the nucleus and the matrix it meets and consumes, until it finally becomes recognizable as a new strain-free crystal separated from its surroundings by a large-angle boundary [9].

Fig.1 shows typical flow curves during cold and hot deformation. During hot deformation, the shape of the flow curve can be 'restricted', or work hardening rates counterbalanced, by dynamic recovery or by dynamic recrystallization (i.e. discontinuous dynamic recrystallization). Dynamic recovery is typical of high-SFE metals (e.g. aluminium, low-carbon ferritic steel, etc.), where the flow stress saturates after an initial period of work hardening. This saturation value depends on temperature, strain rate and composition. On the other hand, as shown in Fig.1, a broad peak (or multiple peaks) typically accompany dynamic recrystallization. Fig.2 illustrates schematically the microstructure developments during dynamic recovery and dynamic recrystallization. During dynamic recovery, the original grains get increasingly strained, but the sub-boundaries remain more or less equiaxed. This implies that the substructure is 'dynamic' and re-adapts continuously to the increasing strain. In low-SFE metals (e.g. austenitic stainless steel, copper, etc.), the process of recovery is slower and this, in turn, may allow sufficient stored energy build-up. At a critical strain, and correspondingly at a value/ variation in driving force, dynamically recrystallized grains appear at the original grain boundaries – resulting in the so-called 'necklace structure'. With further deformation, more and more potential nuclei are activated and new recrystallized grains appear. At the same time, the grains, which had already recrystallized in a previous stage, are deformed again. After a certain amount of strain, saturation/equilibrium sets in (see Fig.2b). Typically equilibrium is reached between the hardening due to dislocation accumulation and the softening due to dynamic recrystallization. At this stage, the flow curve reaches a plateau and the microstructure consist of a dynamic mixture of grains with various dislocation densities. It is important, at this stage, to bring out further the structural developments and structure–property correlation accompanying dynamic recovery and dynamic recrystallization respectively [10].

The true compressive stress-strain curves for as-extruded 7075 aluminum alloy under different temperatures and strain rates are illustrated in Fig. 3a~d. The flow stress as well as the shape of the flow curves is sensitively dependent on temperature and strain rate. Comparing these curves with one another, it is found that increasing strain rate or decreasing deformation temperature makes the flow stress level increase, in other words, it prevents the occurrence of
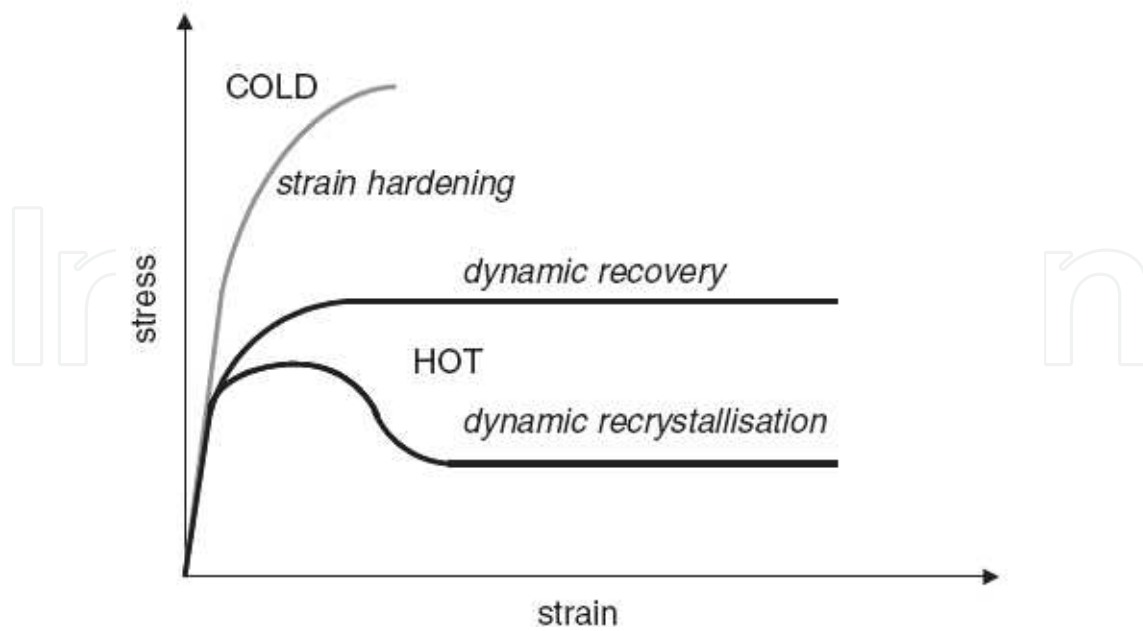
Figure 1. Typical flow curves during cold and hot deformation
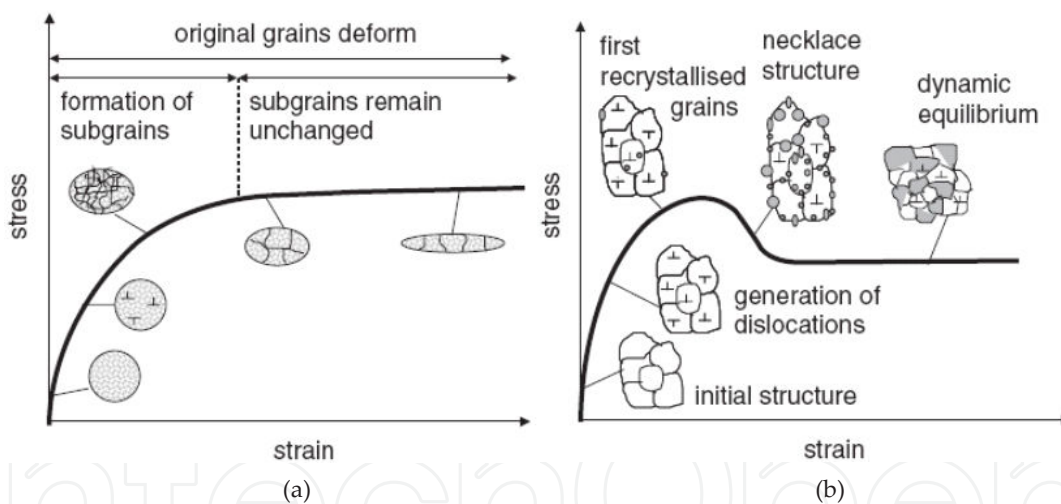

Figure 2. Evolution of the microstructure during (a) hot deformation of a material showing recovery and (b) continuous dynamic recrystallization (CDRX).

softening due to DRX and dynamic recovery (DRV) and makes the deformed metals exhibit work hardening (WH). The cause lies in the fact that higher strain rate and lower temperature provide shorter time for the energy accumulation and lower mobilities at boundaries which result in the nucleation and growth of dynamically recrystallized grains and dislocation annihilation. For every curve, after a rapid increase in the stress to a peak value, the flow stress decreases monotonically towards a steady state regime with a varying softening rate which typically indicates the onset of DRX. In further, from all the true stress-strain curves, it can be summarized that the stress evolution with strain exhibits three distinct stages. At the first stage

where work hardening (WH) predominates, flow stress exhibits a rapid increase to a critical value. At the second stage, flow stress exhibits a smaller and smaller increase until a peak value or an inflection of work-hardening rate, which shows that the thermal softening due to DRX and dynamic recovery (DRV) becomes more and more predominant, then it exceeds WH. At the third stage, two types of curve variation tendency can be generalized as following: decreasing gradually to a steady state with DRX softening (573~723 K & 0.01 s^{-1}, 623~723 K & 0.1 s^{-1}, 623~723 K & 1 s^{-1}, 723 K & 10 s^{-1}), decreasing continuously with significant DRX softening (573 K & 0.1 s^{-1}, 573 K & 1 s^{-1}, 573~623 K & 10 s^{-1}). Thus, it can be concluded that the typical form of flow curve with DRX softening, including a single peak followed by a steady state flow as a plateau, is more recognizable at higher temperatures and lower strain rates. That is because at lower strain rates and higher temperatures, the higher DRX softening rate slows down the rate of work-hardening, and both the peak stress and the onset of steady state flow are therefore shifted to lower strain levels [11].
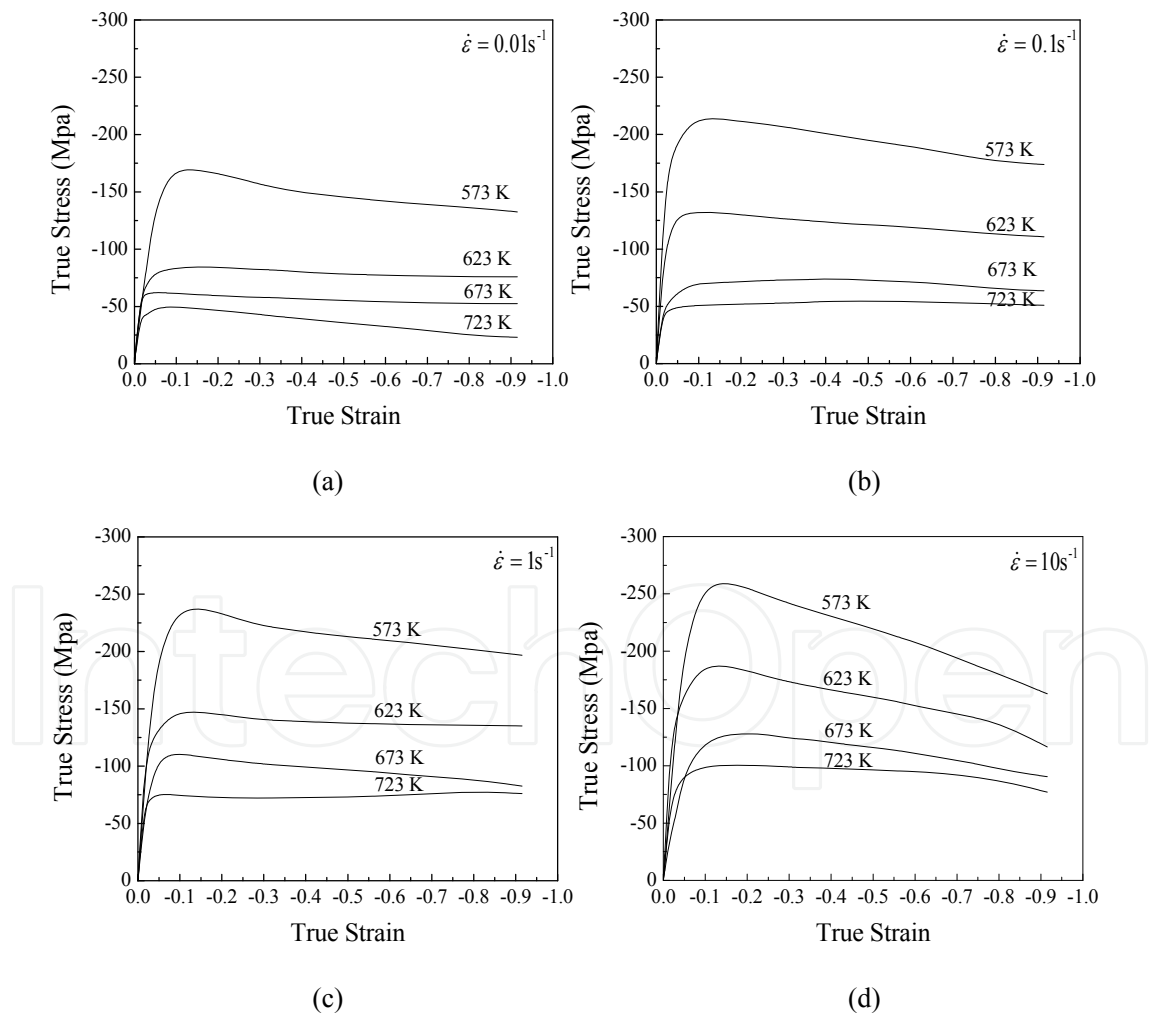

Figure 3. True stress-strain curves of as-extruded 7075 aluminum alloy at different strain rates and temperatures. (a) 0.01 s^{-1}, 573~723 K, (b) 0.1 s^{-1}, 573~723 K, (c) 1 s^{-1}, 573~723 K, (d) 10 s^{-1}, 573~723 K.

The similar flow behavior of as-cast AZ80 magnesium alloy with as-extruded 7075 aluminum alloy is illustrated in Fig. 4a~d. Both deformation temperature and strain rate have considerable influence on the flow stress of AZ80 magnesium alloy. From the true stress-strain curves in Fig. 4a~d, it also can be seen that the stress evolution with strain exhibits three distinct stages. At the first stage where work hardening (WH) predominates and cause dislocations to polygonize into stable subgrains, flow stress exhibits a rapid increase to a critical value with increasing strain, meanwhile the stored energy in the grain boundaries originates from a large difference in dislocation density within subgrains or grains and grows rapidly to DRX activation energy. When the critical driving force is attained, new grains are nucleated along the grain boundaries, deformation bands and dislocations, resulting in equiaxed DRX grains. At the second stage, flow stress exhibits a smaller and smaller increase until a peak value or an inflection of work-hardening rate, which shows that the thermal softening due to DRX and dynamic recovery (DRV) becomes more and more predominant, then it exceeds WH. At the third stage, two types of curve variation tendency can be generalized as following: decreasing gradually to a steady state with DRX softening (573~673 K & 0.01 s^{-1}, 623~673 K & 0.1 s^{-1}, 573 K & 1 s^{-1},, 673 K & 1 s^{-1}), and decreasing continuously with significant DRX softening (523 K & 0.01 s^{-1}, 523~573 K & 0.1 s^{-1}, 523 K & 1 s^{-1},, 623 K & 1 s^{-1}, 523~673 K & 10 s^{-1}) [12-14].
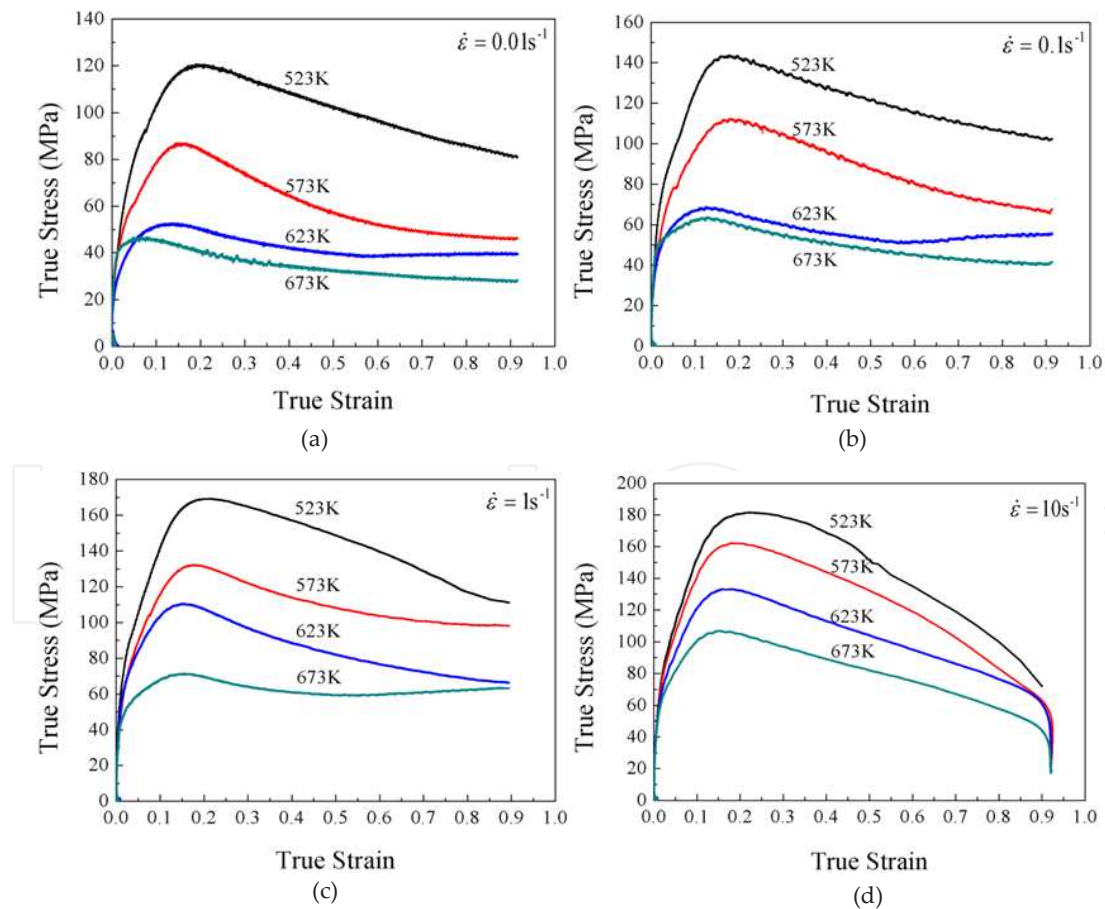

Figure 4. True stress-strain curves of as-cast AZ80 magnesium alloy obtained by Gleeble 1500 under different deformation temperatures with strain rates (a) 0.01 s^{-1}, (b) 0.1 s^{-1}, (c) 1 s^{-1}, (d) 10 s^{-1}.
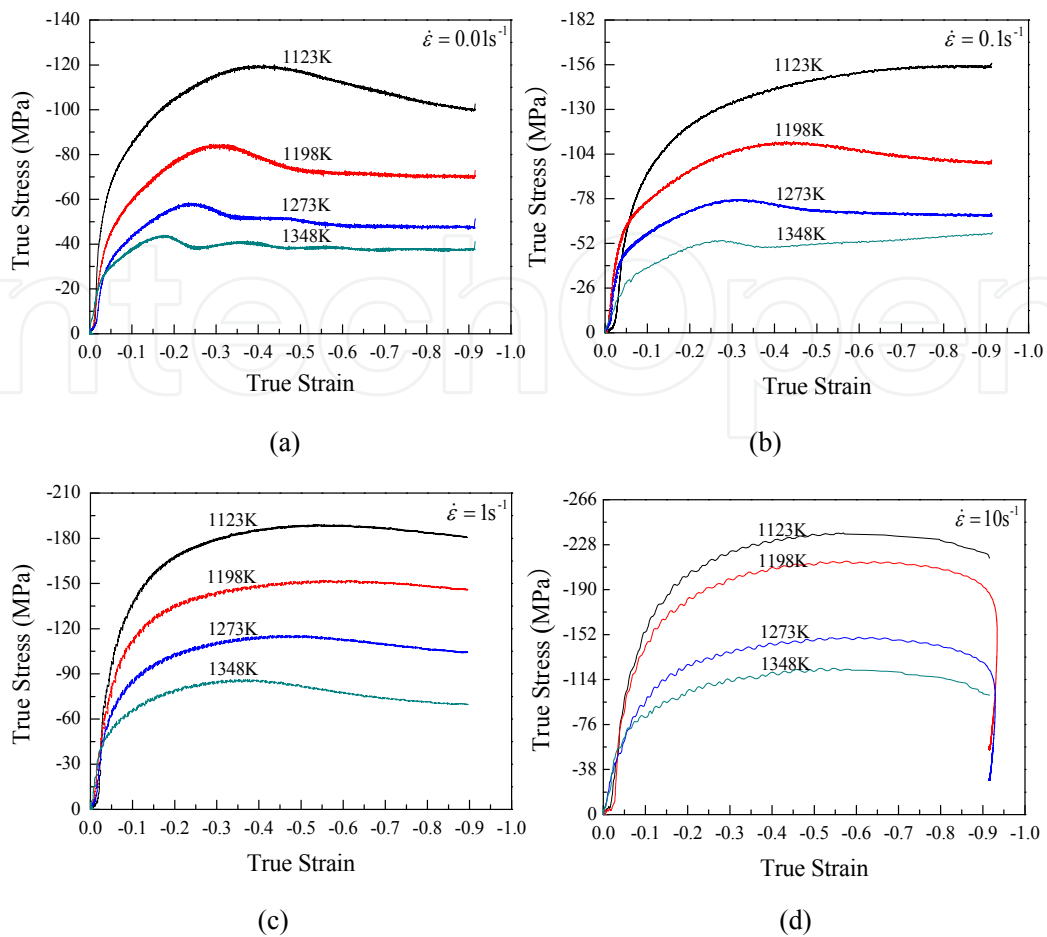
Figure 5. True stress-strain curves of as-extruded 42CrMo high-strength steel obtained by Gleeble 1500 under the different deformation temperatures with strain rates. (a) 0.01 s⁻¹, (b) 0.1 s⁻¹, (c) 1 s⁻¹, (d) 10 s⁻¹.

A little different flow behavior of as-cast 42CrMo high-strength steel from as-extruded 7075 aluminum alloy and as-cast AZ80 magnesium alloy is illustrated in Fig. 5a~d. From the true stress-strain curves in Fig. 5a~d, it also can be seen that the stress evolution with strain exhibits three distinct stages. But the difference is as follows: at the third stage, three types of curve variation tendency can be generalized as following: decreasing gradually to a steady state with DRX softening (1123~1348 K & 0.01 s⁻¹, 1198~1348 K & 0.1 s⁻¹, 1273~1348 K & 1 s⁻¹), maintaining higher stress level without significant softening and work-hardening (1123~1198 K & 1 s⁻¹, 1123~1348 K & 10 s⁻¹), and increasing continuously with significant work-hardening (1123 K & 0.1 s⁻¹) [15-17].

3. DRX critical strain and DRX kinetic model

3.1. The initiation of DRX

From the true compressive stress-strain data of as-extruded 42CrMo high-strength steel shown in Fig. 5a~d, the values of the strain hardening rate ($\theta = d\sigma/d\varepsilon$) were calculated. The critical

conditions for the onset of DRX can be attained when the value of $|-d\theta/d\sigma|$, where strain hardening rate $\theta = d\sigma/d\varepsilon$, reaches the minimum which corresponds to an inflection of $d\sigma/d\varepsilon$ versus σ curve. In this study, analysis of inflections in the plot of $d\sigma/d\varepsilon$ versus σ up to the peak point of the true stress-strain curve has been performed to reveal whether DRX occurs. Results confirm that the $d\sigma/d\varepsilon$ versus σ curves have characteristic inflections as shown in Fig. 6a~d, which indicates that DRX is initiated at corresponding deformation conditions. The critical stress to initiation can be identified, and hence the corresponding critical strain to initiation can be obtained from true stress-strain curve. As a result, the values of critical strain and peak stress at different deformation conditions were shown in Table.1, from which it can be seen that the critical strain and critical stress depend on temperature and strain rate nonlinearly, and it is summarized that $\varepsilon_c/\varepsilon_p = 0.165 \sim 0.572$, $\sigma_c/\sigma_p = 0.645 \sim 0.956$ [15].
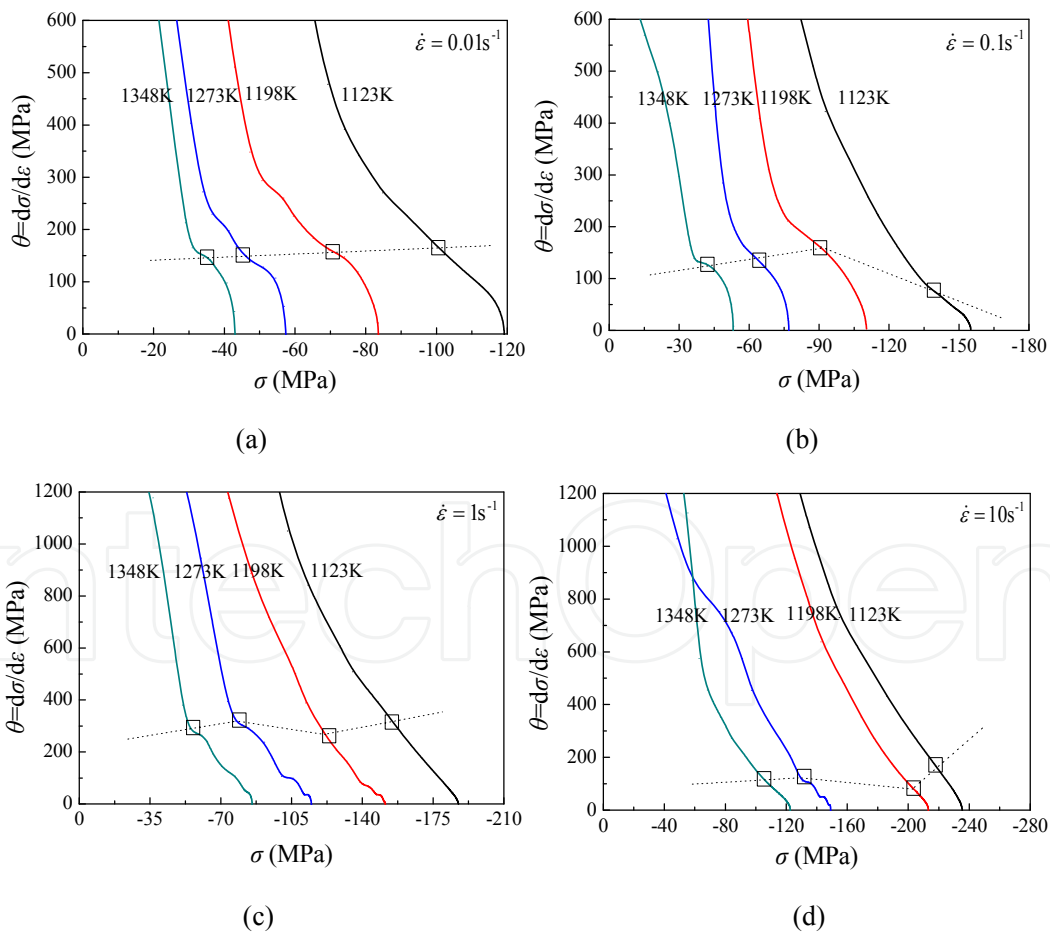

Figure 6. Formula: Eqn012.wmf>versus dσ / dε plots up to the peak points of the true stress-strain curves under differ- ent deformation temperatures with strain rates (a) 0.01 s^{-1}, (b) 0.1 s^{-1}, (c) 1 s^{-1}, (d) 10 s^{-1}.

		Strain rate (s⁻¹)	Temperature (K)			
			1123	1198	1273	1348
True strain	σ	0.01	-0.177	-0.160	-0.113	-0.083
		0.1	-0.336	-0.172	-0.140	-0.142
		1	-0.146	-0.135	-0.077	-0.059
		10	-0.259	-0.359	-0.247	-0.218
	ε_c	0.01	-0.400	-0.309	-0.236	-0.355
		0.1	-0.818	-0.436	-0.318	-0.264
		1	-0.545	-0.591	-0.455	-0.355
		10	-0.564	-0.627	-0.600	-0.573
True stress (MPa)	ε_p	0.01	-100.875	-70.523	-45.244	-35.122
		0.1	-137.038	-89.748	-63.469	-42.362
		1	-153.988	-122.629	-76.918	-55.127
		10	-215.180	-203.734	-131.429	-105.296
	σ_c	0.01	-119.111	-83.558	-57.221	-40.714
		0.1	-155.026	-110.287	-77.083	-53.280
		1	-187.522	-151.374	-114.790	-85.495
		10	-235.405	-213.198	-149.191	-122.623
σ_p		0.01	0.441	0.519	0.476	0.234
		0.1	0.411	0.394	0.439	0.540
		1	0.268	0.229	0.170	0.165
		10	0.459	0.572	0.412	0.381
$\varepsilon_c / \varepsilon_p$		0.01	0.847	0.844	0.791	0.863
		0.1	0.884	0.814	0.823	0.795
		1	0.821	0.810	0.670	0.645
		10	0.914	0.956	0.881	0.859

Table 1. Values of σ_c / σ_p, ε_c, σ_c and ε_p at different deformation conditions.

3.2. Arrhenius equation for flow behavior with DRX

It is known that the thermally activated stored energy developed during deformation controls softening mechanisms which induce different DRX softening and work-hardening. The activation energy of DRX, an important material parameter, determines the critical conditions for DRX initiation. So far, several empirical equations have been proposed to determine the deformation activation energy and hot deformation behavior of metals. The most frequently used one is Arrhenius equation which designs a famous Zener-Hollomon parameter, σ_p, to

represent the effects of the temperatures and strain rate on the deformation behaviors, and then uncovers the approximative hyperbolic law between Z parameter and flow stress [15].

$$Z = \dot{\varepsilon} \exp(Q/RT) \tag{1}$$

$$\dot{\varepsilon} = AF(\sigma) \exp(-Q/RT) \tag{2}$$

Where,

where $F(\sigma) = \begin{cases} |\sigma|^n & \alpha |\sigma| < 0.8 \\ \exp(\beta |\sigma|) & \alpha |\sigma| > 1.2 \\ [\sinh(\alpha |\sigma|)]^n & \text{for all } \sigma \end{cases}$ is the strain rate (s^{-1}), $\dot{\varepsilon}$ is the universal gas constant (8.31 J mol^{-1} K^{-1}), R is the absolute temperature (K), T is the activation energy of DRX (kJ mol^{-1}), Q is the flow stress (MPa) for a given stain, σ, A and α are the material constants (n).

3.2.1. Calculation of material constant $\alpha = \beta / n$

For the low stress level (n), substituting the power law of $\alpha\sigma < 0.8$ into Eq. (2) and taking natural logarithms on both sides of Eq. (2) give

$$\ln \dot{\varepsilon} = \ln A + n \ln |\sigma| - Q/RT \tag{3}$$

Then, $\ln\dot{\varepsilon} = \ln A + n \ln |\sigma| - Q/RT$. In 2010, Quan et al. [17] plotted the relationships between the true stress and true strain of 42CrMo high-strength steel in ln-ln scale under different temperatures and strain rates, and hence found a true strain range of -0.08~-0.18 including part of the first stage and the second stage described in the previous, in which all the stresses increase gradually with almost the same ratios. Therefore, this true strain range was accepted as a steady WH stage corresponding to low stress level. In further, Quan et al. [17] fitted the relationships between the stress and the strain rate as the true strain was -0.14, and then found almost equally linear relationships which revealed that the influence of temperature was very small. Thus, it can be deduced that to evaluate the material constant $n = d\ln\dot{\varepsilon} / d\ln |\sigma|$ of Arrhenius equation, the stress-strain data in the true strain range of -0.08~-0.18 contribute to the minimum calculation tolerance. Here true strain n was chose. Fig. 7 shows the relationships between $\varepsilon = -0.1$ and $\ln |\sigma|$ for $\ln\dot{\varepsilon}$ under different temperatures. The linear relationship is observed for each temperature and the slope rates are almost similar with each other. The mean value of all the slope rates is accepted as the inverse of material constant $\varepsilon = -0.1$, thus n value is obtained as 8.27780.

3.2.2. Calculation of material constant $\ln\dot{\varepsilon}$

For the high stress level (β), substituting the exponential law of $\alpha |\sigma| > 1.2$ into Eq. (2) and taking natural logarithms on both sides of Eq. (2) give
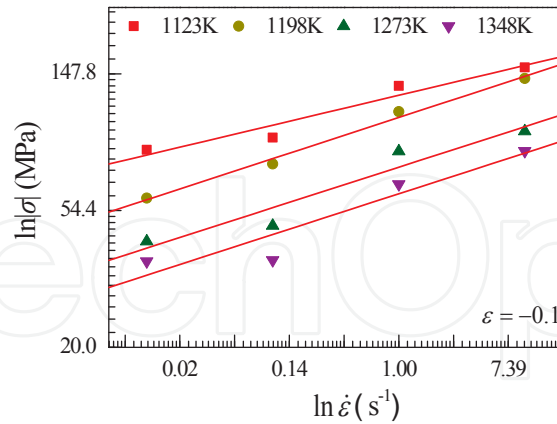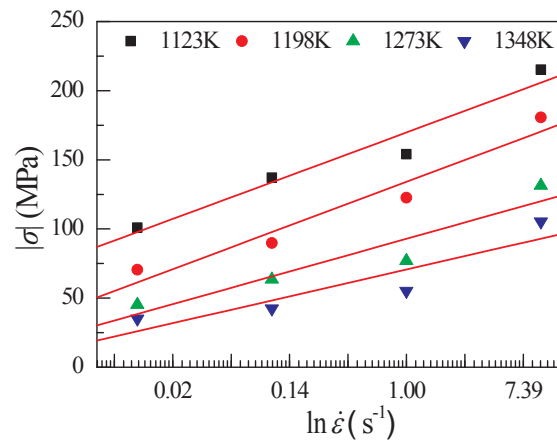
Figure 7. The relationships between n and $\ln\sigma$.

Figure 8. The relationships between $\alpha = \beta / n = 0.00913$ and $|\sigma|$.

$$\ln\dot{\varepsilon} = \ln A + \beta|\sigma| - Q/RT \qquad (4)$$

Then, $\ln\dot{\varepsilon} = \ln A + \beta|\sigma| - Q/RT$. The peak stresses at different temperatures and strain rates can be identified for the target stresses with high level. The linear relationships between $\beta = d\ln\dot{\varepsilon}/|\sigma|$ and $|\sigma|$ at different temperatures were fitted out as Fig. 8. The mean value of all the slope rates is accepted as the inverse of material constant $\ln\dot{\varepsilon}$, thus β value is obtained as 0.07558 MPa⁻¹. Thus, another material constant β MPa⁻¹.

3.2.3. Calculation of DRX activation energy $\ln\dot{\varepsilon}$

For all the stress level (including low and high stress levels), Eq.(2) can be represented as the following

$$\ln\dot{\varepsilon} = \ln A + n\left[\ln\sinh(\alpha|\sigma|)\right] - Q/RT \tag{5}$$

If $\ln\dot{\varepsilon} = \ln A + n[\ln\sinh(\alpha|\sigma|)] - Q/RT$ is constant, there is a linear relationship between $\dot{\varepsilon}$ and $\ln\sinh(\alpha|\sigma|)$, and Eq. (5) can be rewritten as

$$Q = Rn\left\{d\left[\ln\sinh(\alpha|\sigma|)\right]/d(1/T)\right\} \tag{6}$$

The peak stresses at different temperatures and strain rates can be identified for the present target stresses. The linear relationships between $Q = Rn\{d[\ln\sinh(\alpha|\sigma|)]/d(1/T)\}$ and $\ln\sinh(\alpha\sigma)$ at different strain rates were fitted out as Fig. 9. The mean value of all the slope rates is accepted as $1/T$ value, then Q/Rn is calculated as 599.73210 kJ mol^{-1}. The activation energy of DRX is a term defined as the energy that must be overcome in order for the nucleation and growth of new surface or grain boundary to occur. In 2008, Lin et al. found that the activation energy of as-cast 42CrMo steel is not a constant but a variable 392~460 kJ mol^{-1} as a function of strain, and the peak value of DRX energy corresponds to the peak stress [18, 19]. In this investigate, the influence of strain on the variable activation energy was ignored to simplify the following calculations, and only the peak value of DRX energy was accepted as the activation energy of DRX. This simplification ensures the predicted occurrence of DRX by the derived equations. Lin et al. also pointed that the average value of the activation energy of as-cast 42CrMo steel is 438.865 kJ mol^{-1} [18, 19]. The average Q value of extruded 42CrMo steel, 599.73210 kJ mol^{-1}, is a little higher than that of as-cast 42CrMo steel adopted by Lin et al. The difference of two average Q values results from the different as-received statuses. In common, the higher deformation activation energy will be found in hot deformation of as-received steels with higher yield strength. It is obvious that the true stress data of extruded rods in this work are higher than that of as-cast billets in the work of Lin et al. In addition, the difference of experiment projects involving strain rate between this work and the work of Lin et al is another important reason for the difference of calculation result.
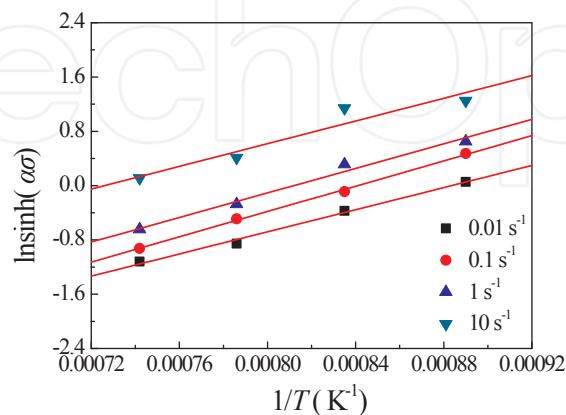

Figure 9. The relationships between Q and $\ln\sinh(\alpha|\sigma|)$.

3.2.4. Construction of constitutive equation

Substituting $1/T$, α, n and four sets of Q, $\dot{\varepsilon}$ and T into Eq. (5), the mean value of material constant σ is obtained as 2.44154×10^{25} s⁻¹. Thus, the relationship between A, $\dot{\varepsilon}$ and T can be expressed as

$$\dot{\varepsilon} = 2.44154 \times 10^{25} \left[\sinh(0.00913|\sigma|)^{8.27780} \right] \exp\left[-(599.73210 \times 10^3)/8.31T \right] \qquad (7)$$

Substituting $\dot{\varepsilon} = 2.44154 \times 10^{25} [\sinh(0.00913|\sigma|)^{8.27780}] \exp[-(599.73210 \times 10^3)/8.31T]$ into Eq. (7), thus, the the flow stress can be expressed as

$$|\sigma| = 109.52903 \ln\left\{ [Z/(2.44154 \times 10^{25})]^{1/8.27780} + \{[Z/(2.44154 \times 10^{25})]^{2/8.27780} + 1\}^{1/2} \right\} \qquad (8)$$

3.3. DRX kinetic model

During thermoplastic deformation process, dislocations continually increase and accumulate to such an extent that at a critical strain, DRX nucleus would form and grow up near grain boundaries, twin boundaries and deformation bands. It is well known that the conflicting effects coexist between the multiplication of dislocation due to continual hot deformation and the annihilation of dislocation due to DRX. When work-hardening corresponding to the former and DRX softening corresponding to the later are in dynamic balance, flow stress will keep constant with increasing strain, meanwhile deformation comes to a steady stage in which complete DRX grains have equiaxed shape and keep constant size. In common, the kinetics of DRX can be described in terms of normal S-curves of the recrystallized volume expressed as a function of time. In a constant strain rate, time can be replaced by strain and recrystallized volume fraction can be expressed by modified Avrami equation. Thus, the kinetics of DRX evolution can be predicted by the following equation [20].

$$X_{\text{DRX}} = 1 - \exp\left\{ -\left[(\varepsilon - \varepsilon_c)/\varepsilon^* \right]^m \right\} \qquad (9)$$

where $X_{\text{DRX}} = 1 - \exp\{ -[(\varepsilon - \varepsilon_c)/\varepsilon^*]^m \}$ is the volume fraction of dynamic recrystallized grain and X_{DRX} is Avrami's constant. This expression, which is modified from the Avrami's equation, means that m depends on strain, strain rate and temperature.

The true stress-strain curve data after the peak stress point were adopted to calculate DRX softening rate (X_{DRX} versus $\theta = \text{d}\sigma/\text{d}\varepsilon$) plots, and the results were shown as Fig. 10a~d. The maximum softening rate corresponds to the negative peak of such plot. The strain for maximum softening rate, σ, identified from Fig. 10a~d, and the critical strain, ε^*, identified from Fig. 10a~d can be considered with a power function of dimensionless parameter, ε_c (Fig. 11a~b).

The function expressions linearly fitted by the method of least squares are Z/A and

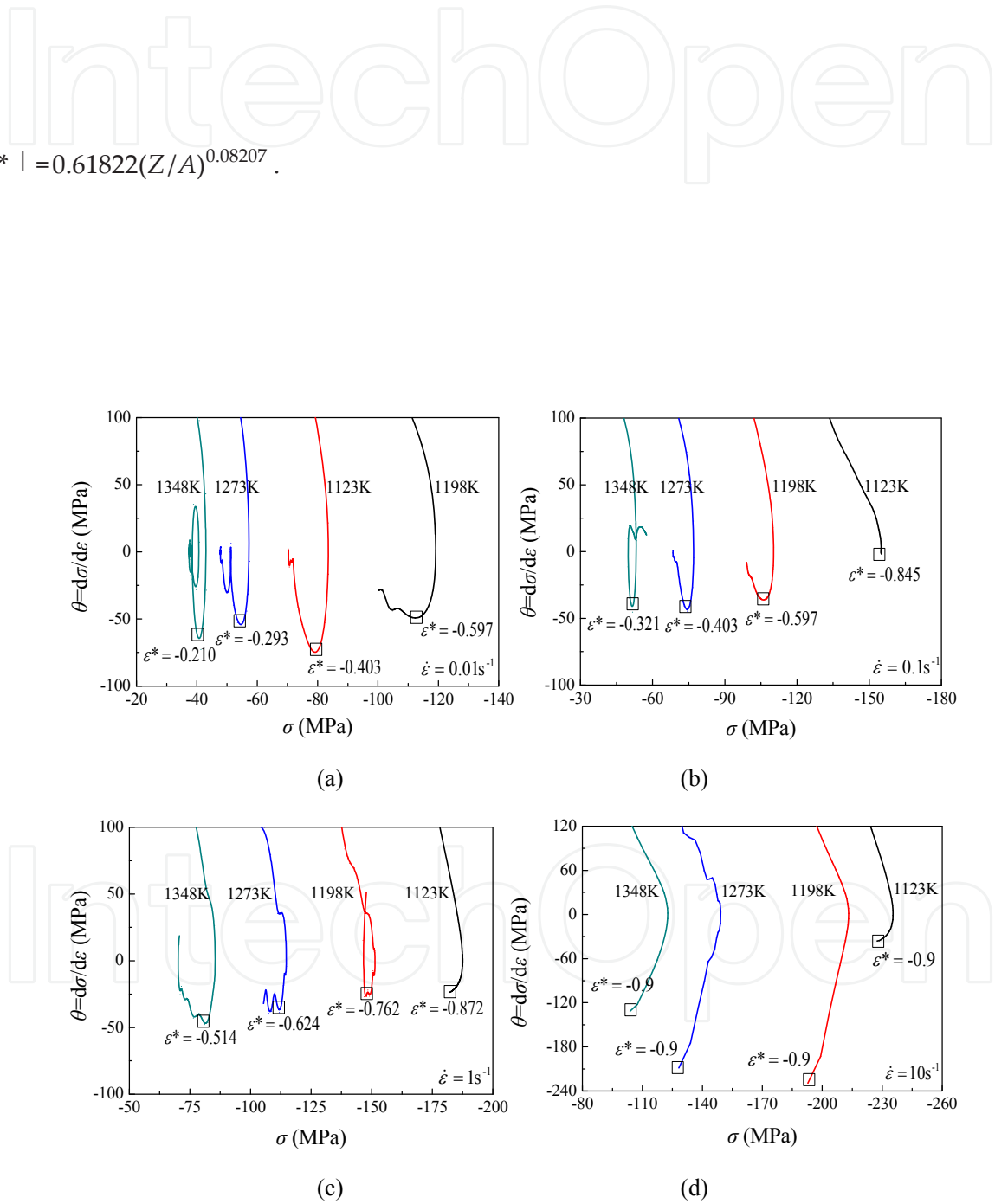$$|\varepsilon*| = 0.61822(Z/A)^{0.08207}.$$

Figure 10. Formula: Eqn102.wmf>versus $|\varepsilon_c| = 0.16707(Z/A)^{0.06704}$ plots after the peak points of the true stress-strain curves under different deformation temperatures with strain rates (a) 0.01 s^{-1}, (b) 0.1 s^{-1}, (c) 1 s^{-1}, (d) 10 s^{-1}.
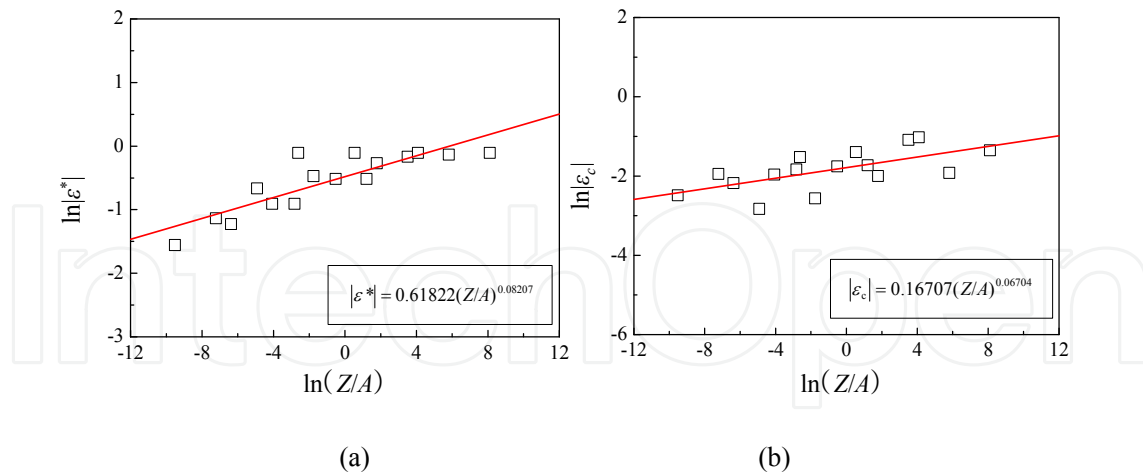
Figure 11. Relationships between the dimensionless parameter, Z/A, and (a) dσ / dε , (b) σ .

In order to solve the Avrami's constant, $\varepsilon *$, it is essential to identify the deformation conditions corresponding to ε_c meaning that the flow stress reaches a steady state in which complete DRX grains have equiaxed shape and keep constant size. From the true compressive stress-strain curves in Fig. 5a~d, and m versus $X_{DRX} = 1$ plots in Fig. 10a~d, such the deformation conditions can be identified as shown in Table.2. Substituting these deformation conditions corresponding to dσ / dε into Eq. (9), the mean value of the Avrami's constant σ can be obtained as 3.85582. Thus, the kinetic model of DRX calculated from true compressive stress-strain curves can be expressed as Table.3.

True strain	Temperature (K)	Strain rate (s⁻¹)
-0.5~-0.9	1198	0.01
-0.4~-0.9	1273	0.01
-0.3~-0.9	1348	0.01
-0.6~-0.9	1273	0.1
-0.4~-0.9	1348	0.1

Table 2. The deformation strain corresponding to $X_{DRX} = 1$.

Volume fractions of dynamic recrystallization	Exponents
m	$X_{DRX} = 1$
	$X_{DRX} = 1 - \exp\{-[(\varepsilon - \varepsilon_c) / \varepsilon *]^m\}$
	$\|\varepsilon *\| = 0.61822(Z / A)^{0.08207}$
	$\|\varepsilon_c\| = 0.16707(Z / A)^{0.06704} s^{-1}$

Volume fractions of dynamic recrystallization	Exponents
	$Z = \dot{\varepsilon} \exp[(599.73210 \times 10^3) / 8.31T]$

Table 3. The kinetic model of DRX calculated from true compressive stress-strain curves.

Based on the calculation results of this model, the effect of deformation temperature, strain and strain rate on the recrystallized volume fraction is shown in Fig. 12a~d. These figures show that as the strain' absolute value increases, the DRX volume fraction increases and reaches a constant value of 1 meaning the completion of DRX process. Comparing these curves with one another, it is found that, for a specific strain rate, the deformation strain required for the same amount of DRX volume fraction increases with decreasing deformation temperature, which means that DRX is delayed to a longer time. In contrast, for a fixed temperature, the deformation strain required for the same amount of DRX volume fraction increases with increasing strain rate, which also means that DRX is delayed to a longer time. This effect can be attributed to decreased mobility of grain boundaries (growth kinetics) with increasing strain rate and decreasing temperature. Thus, under higher strain rates and lower temperatures, the deformed metal tends to incomplete DRX, that is to say, the DRX volume fraction tends to be less than 1.
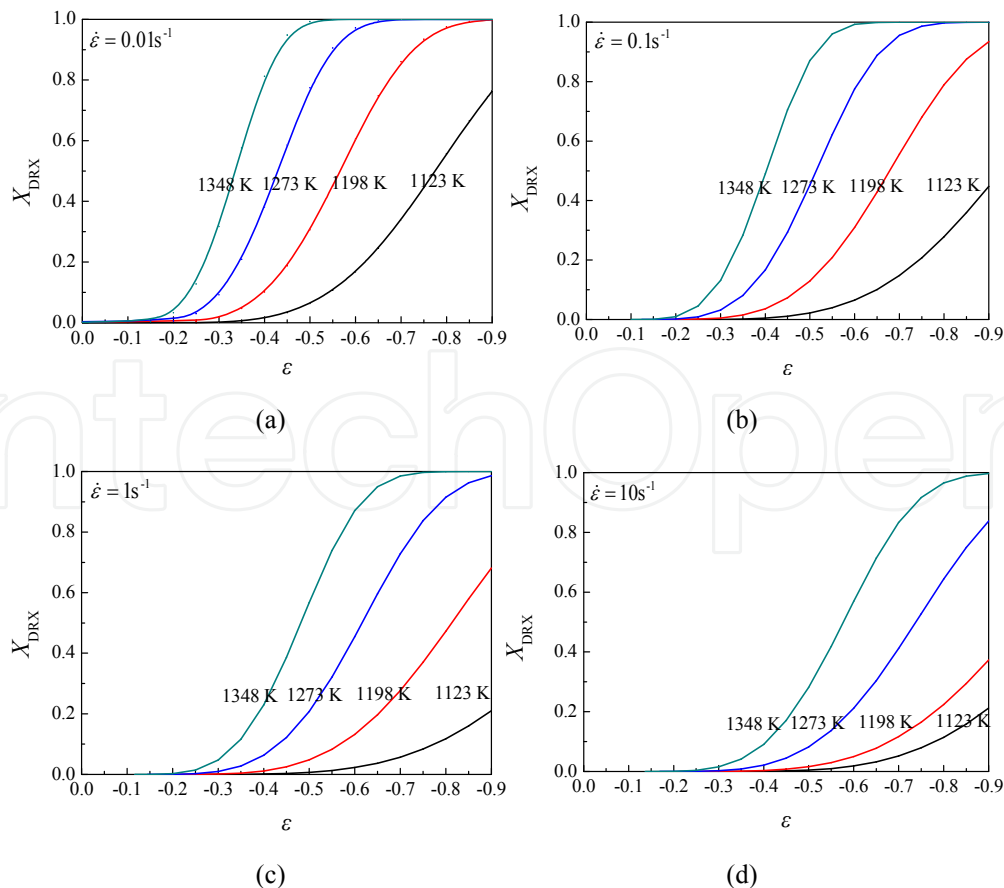

(a)

(b)

(c)

(d)

Figure 12. Predicted volume fractions of dynamic recrystallization obtained under different deformation temperatures with strain rates (a) 0.01 s^{-1}, (b) 0.1 s^{-1}, (c) 1 s^{-1}, (d) 10 s^{-1}.

4. Observation for size and fraction of DRX grains

The microstructures on the section plane of specimen deformed to the true strain of -0.9 were examined and analyzed under the optical microscope. Fig. 13 shows the as-received microstructure of as-extruded 42CrMo high-strength steel specimen with a single-phase FCC structure and a homogeneous aggregate of rough equiaxed polygonal grains, while with negligible volume fraction of inclusions or second-phase precipitates. The grain boundaries are straight to gently curved and often intersect at ~120° triple junctions. Fig. 14a~d show the typical microstructures of the specimens of as-extruded 42CrMo high-strength steel deformed to a strain of -0.9 at the temperature of 1123 K and at the strain rates of 0.01 s^{-1}, 0.1 s^{-1}, 1 s^{-1} and 10 s^{-1}, respectively. Fig. 15a~d show the typical microstructures of the specimens of as-extruded 42CrMo high-strength steel deformed to a strain of -0.9 at the temperature of 1198 K and at the strain rates of 0.01 s^{-1}, 0.1 s^{-1}, 1 s^{-1} and 10 s^{-1}, respectively. Fig. 16a~d show the typical microstructures of the specimens of as-extruded 42CrMo high-strength steel deformed to a strain of -0.9 at the temperature of 1273 K and at the strain rates of 0.01 s^{-1}, 0.1 s^{-1}, 1 s^{-1} and 10 s^{-1}, respectively. Fig. 17a~d show the typical microstructures of the specimens of as-extruded 42CrMo high-strength steel deformed to a strain of -0.9 at the temperature of 1348 K and at the strain rates of 0.01 s^{-1}, 0.1 s^{-1}, 1 s^{-1} and 10 s^{-1}, respectively. At such deformation conditions the recrystallized grains with wavy or corrugated grain boundaries can be easily identified from subgrains by the misorientation between adjacent grains, i.e. subgrains are surrounded by low angle boundaries while recrystallized grains have high angle boundaries. The deformed metal completely or partially transforms to a microstructure of approximately equiaxed defect-free grains which are predominantly bounded by high angle boundaries (i.e. a recrystallized microstructure) by relatively localized boundary migration.
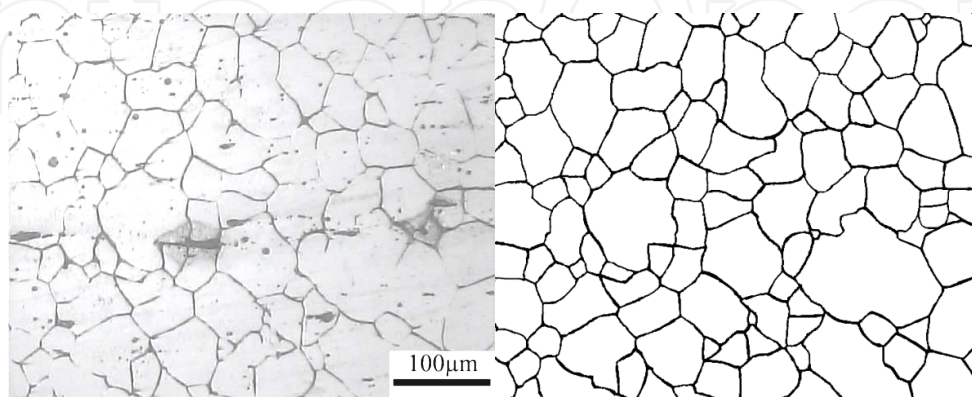

Figure 13. Optical microstructures and average grain size of as-extruded 42CrMo high-strength steel undeformed (starting material)
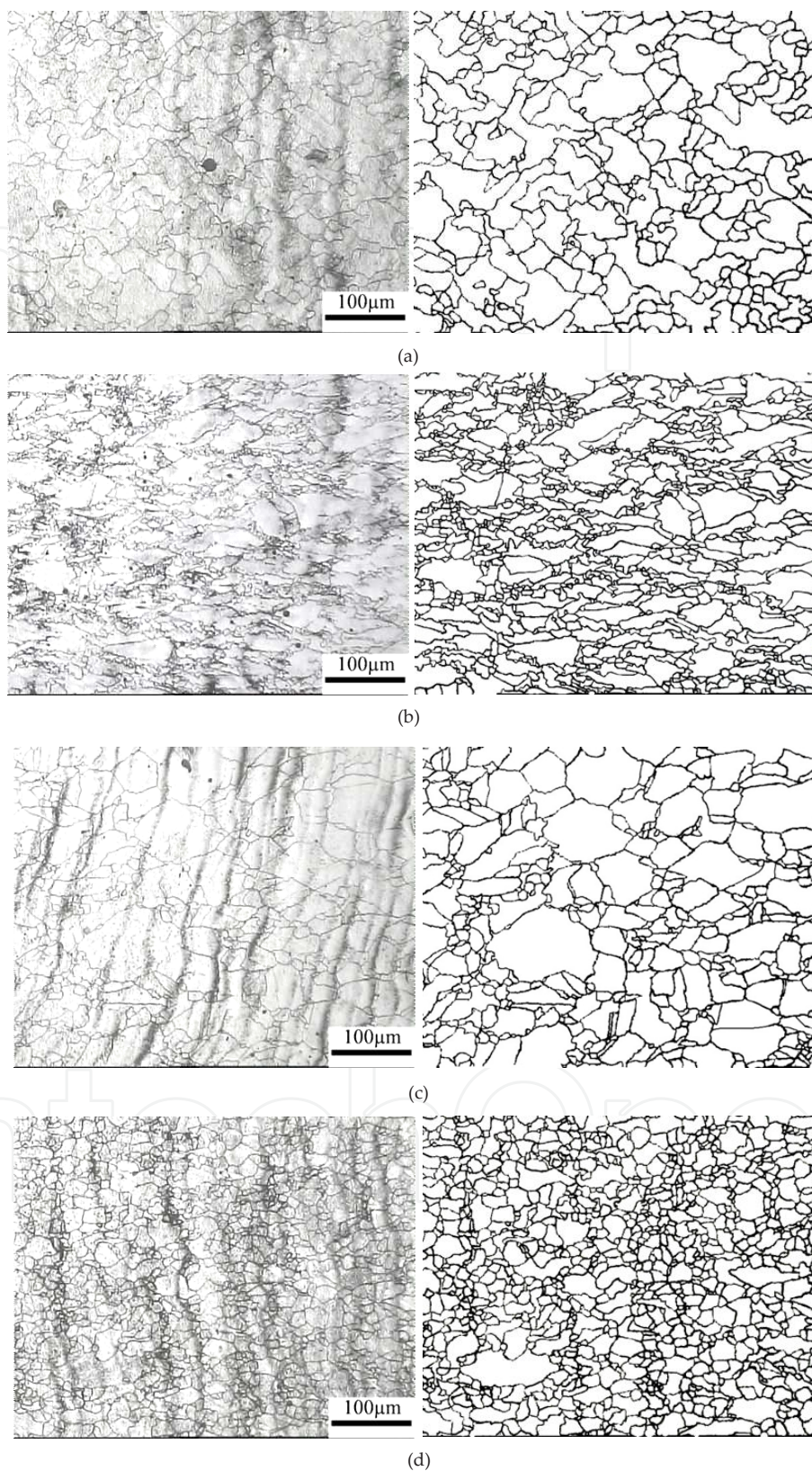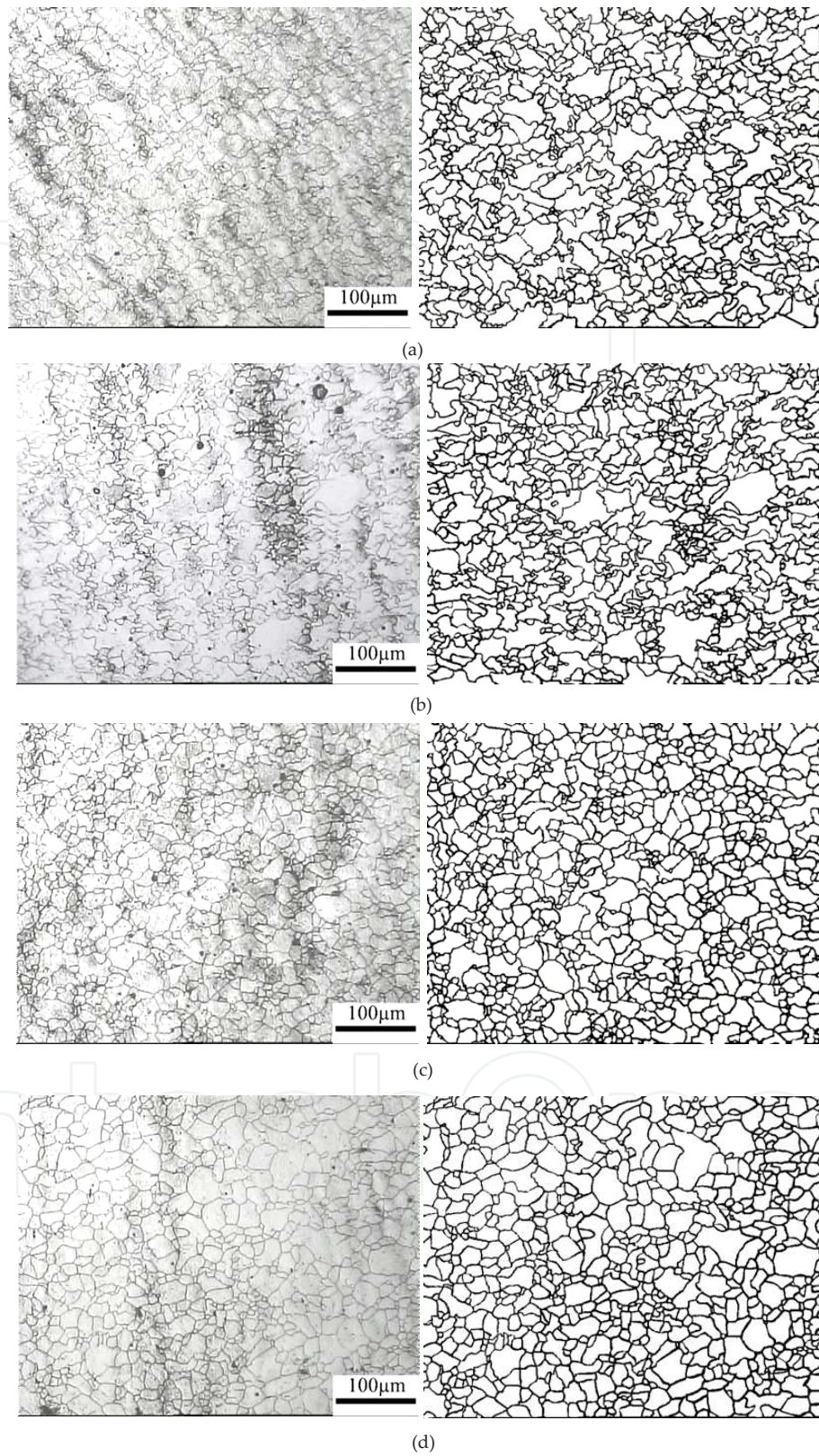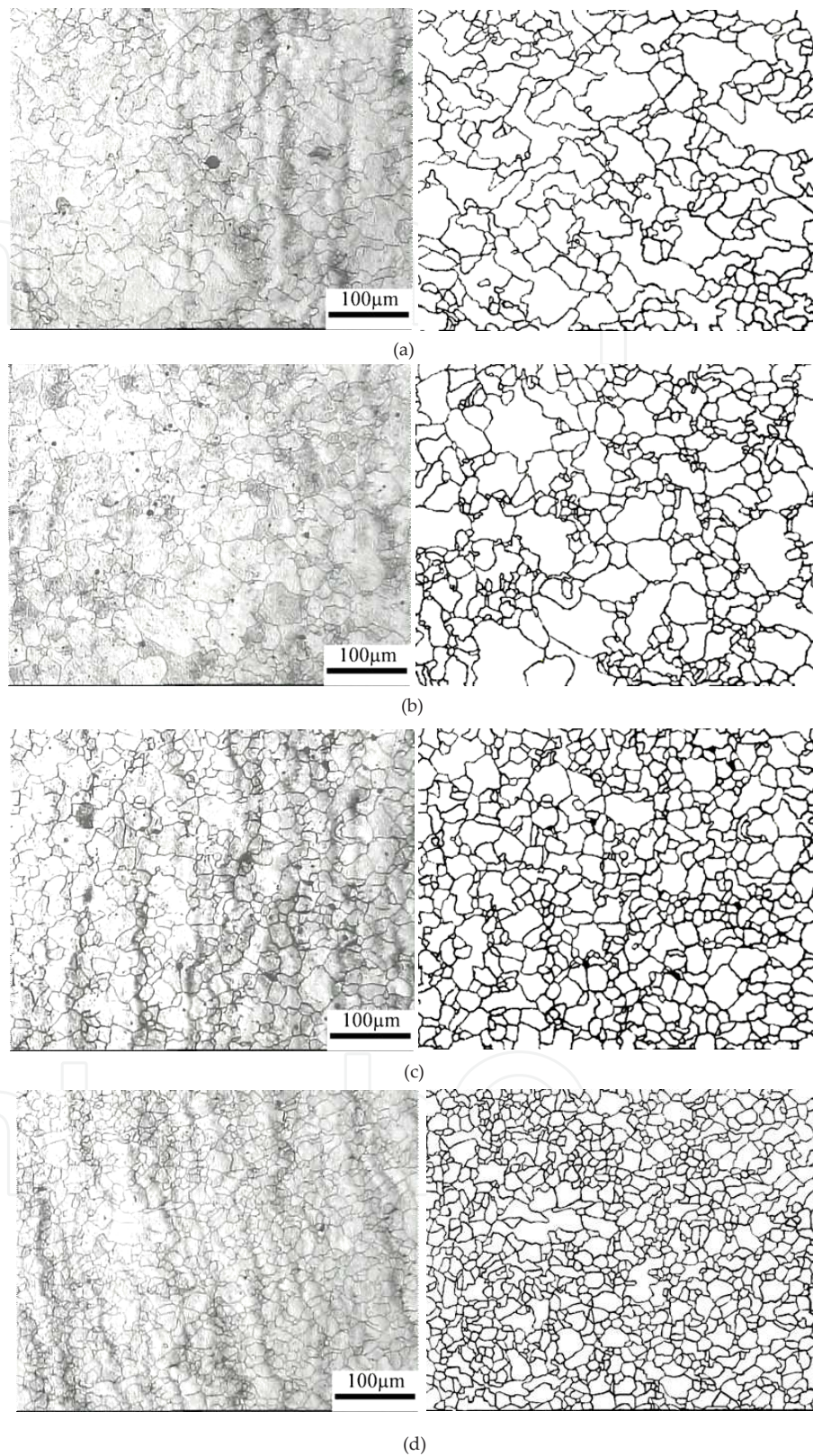
(a)

(b)

(c)

(d)

Figure 14. Optical microstructures of 42CrMo high-strength steel at a fix true strain of 0.9, a fix temperature of 1123 K and different strain rates: (a) 0.01 s^{-1}, (b) 0.1 s^{-1}, (c) 1 s^{-1}, (d) 10 s^{-1}.
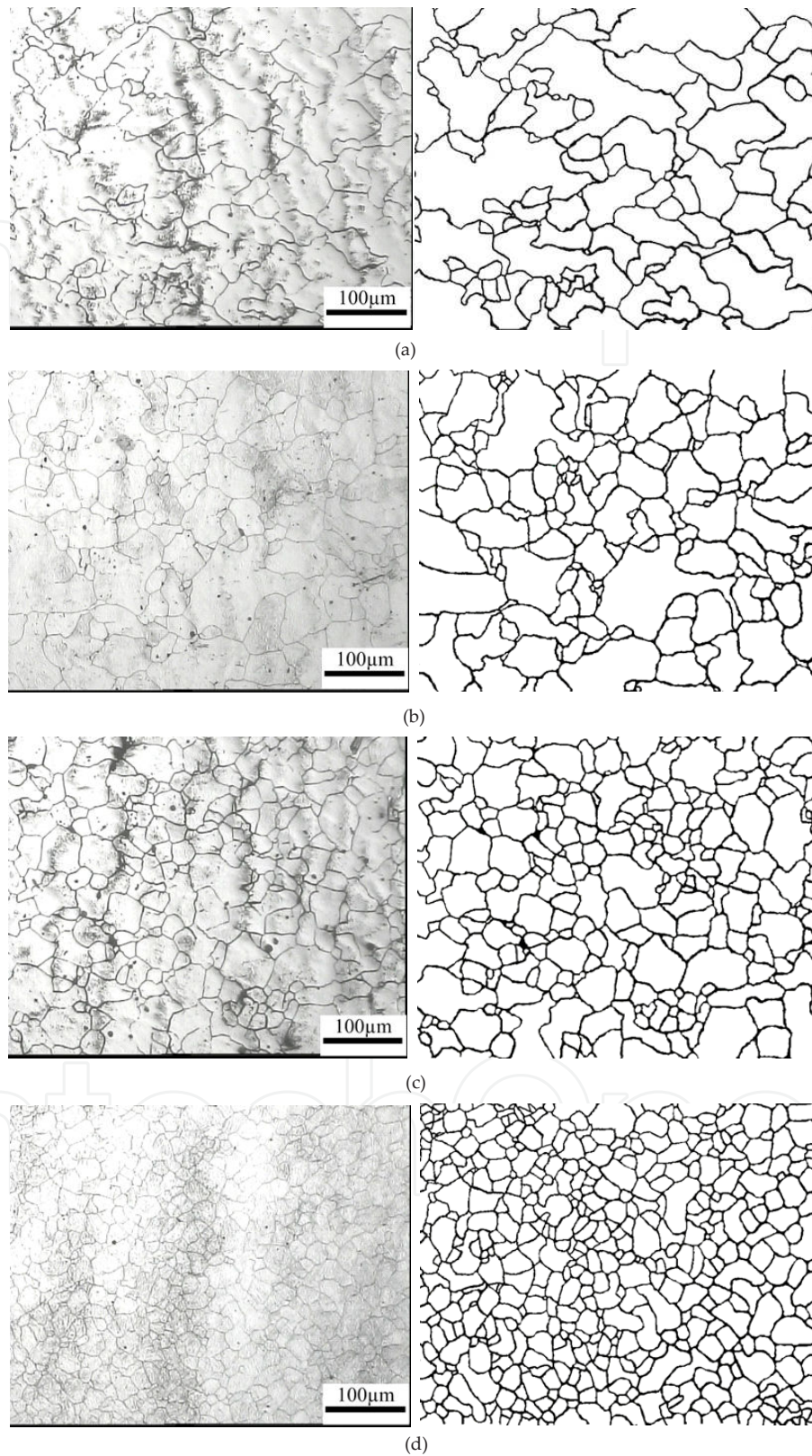
(a)

(b)

(c)

(d)

Figure 15. Optical microstructures of 42CrMo high-strength steel at a fix true strain of 0.9, a fix temperature of 1198 K and different strain rates: (a) 0.01 s^{-1}, (b) 0.1 s^{-1}, (c) 1 s^{-1}, (d) 10 s^{-1}.

(a)

(b)

(c)

(d)

Figure 16. Optical microstructures of 42CrMo high-strength steel at a fix true strain of 0.9, a fix temperature of 1273 K and different strain rates: (a) 0.01 s^{-1}, (b) 0.1 s^{-1}, (c) 1 s^{-1}, (d) 10 s^{-1}.

(a)

(b)

(c)

(d)

Figure 17. Optical microstructures of 42CrMo high-strength steel at a fix true strain of 0.9, a fix temperature of 1348 K and different strain rates: (a) 0.01 s^{-1}, (b) 0.1 s^{-1}, (c) 1 s^{-1}, (d) 10 s^{-1}.

Fig. 18 shows the grain size distribution of as-extruded 42CrMo high-strength steel undeformed (starting material). Fig. 19 shows the grain size distribution of 42CrMo high-strength steel at a fix true strain of 0.9, a fix temperature of 1123 K and different strain rates: (a) 0.01 s^{-1}, (b) 0.1 s^{-1}, (c) 1 s^{-1}, (d) 10 s^{-1}. Fig. 20 shows the grain size distribution of 42CrMo high-strength steel at a fix true strain of 0.9, a fix temperature of 1198 K and different strain rates: (a) 0.01 s^{-1}, (b) 0.1 s^{-1}, (c) 1 s^{-1}, (d) 10 s^{-1}. Fig. 21 shows the grain size distribution of 42CrMo high-strength steel at a fix true strain of 0.9, a fix temperature of 1273 K and different strain rates: (a) 0.01 s^{-1}, (b) 0.1 s^{-1}, (c) 1 s^{-1}, (d) 10 s^{-1}. Fig. 22 shows the grain size distribution of 42CrMo high-strength steel at a fix true strain of 0.9, a fix temperature of 1348 K and different strain rates: (a) 0.01 s^{-1}, (b) 0.1 s^{-1}, (c) 1 s^{-1}, (d) 10 s^{-1}. As depicted, under a fix temperature of 1123 K the microstructure of the as-cast billet with grain size of 53.1 μm became refined up to about 30.1 μm after upsetting under strain rate 0.01 s^{-1}, to about 25.4 μm under strain rate 0.1 s^{-1}, to about 20.4 μm under strain rate 1 s^{-1}, to about 15.6 μm under strain rate 10 s^{-1}. Under a fix temperature of 1198 K the microstructure of the as-cast billet with grain size of 53.1 μm became refined up to about 33.5 μm after upsetting under strain rate 0.01 s^{-1}, to about 26.9 μm under strain rate 0.1 s^{-1}, to about 21.0 μm under strain rate 1 s^{-1}, to about 18.5 μm under strain rate 10 s^{-1}. Under a fix temperature of 1273 K the microstructure of the as-cast billet with grain size of 53.1 μm became refined up to about 33.5 μm after upsetting under strain rate 0.01 s^{-1}, to about 27.3 μm under strain rate 0.1 s^{-1}, to about 19.7 μm under strain rate 1 s^{-1}, to about 15.7 μm under strain rate 10 s^{-1}. Under a fix temperature of 1348 K the microstructure of the as-cast billet with grain size of 53.1 μm became refined up to about 49.8 μm after upsetting under strain rate 0.01 s^{-1}, to about 38.2 μm under strain rate 0.1 s^{-1}, to about 32.2 μm under strain rate 1 s^{-1}, to about 24.4 μm under strain rate 10 s^{-1}. It can be summarized that under a fix temperature, as deformation strain rate increases, the microstructure of the as-received billet becomes more and more refined due to increasing migration energy stored in grain boundaries and decreasing grain growth time.
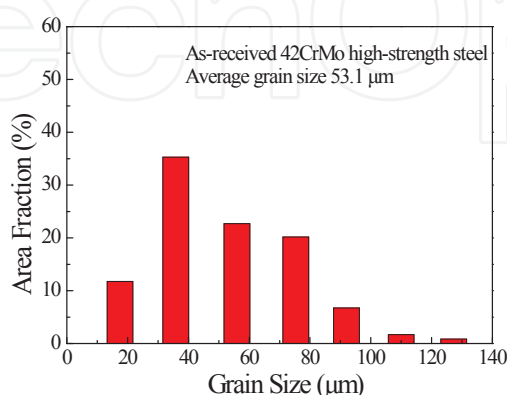

Figure 18. Grain size distribution of as-extruded 42CrMo high-strength steel undeformed (starting material).
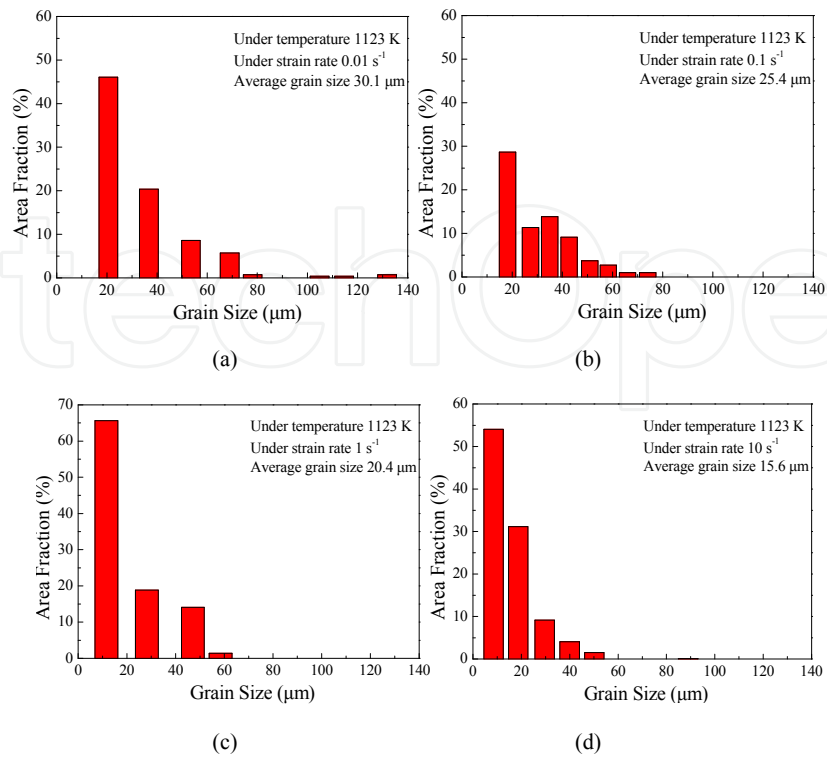
Figure 19. Grain size distribution of 42CrMo high-strength steel at a fix true strain of 0.9, a fix temperature of 1123 K and different strain rates: (a) 0.01 s^{-1}, (b) 0.1 s^{-1}, (c) 1 s^{-1}, (d) 10 s^{-1}.
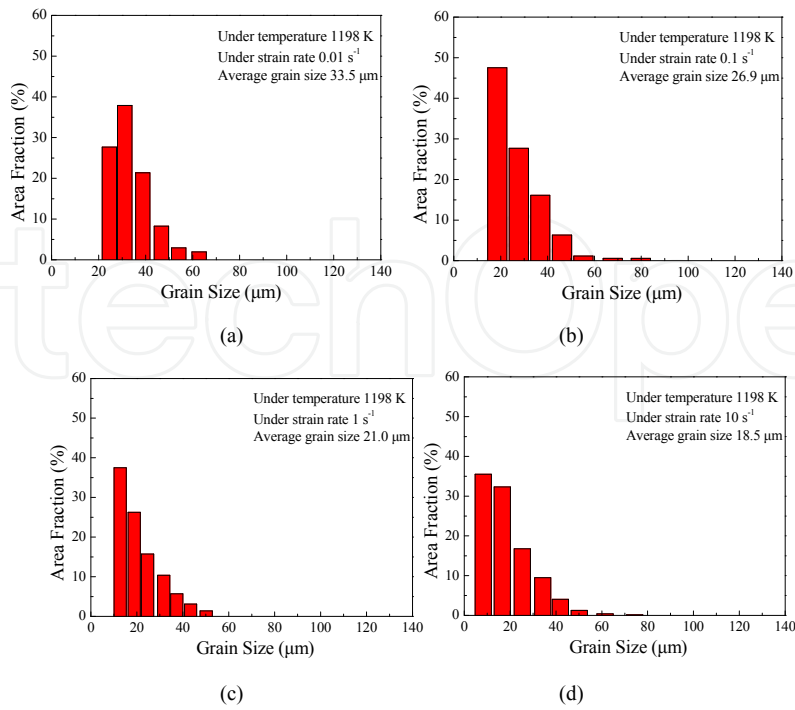
Figure 20. Grain size distribution of 42CrMo high-strength steel at a fix true strain of 0.9, a fix temperature of 1198 K and different strain rates: (a) 0.01 s⁻¹, (b) 0.1 s⁻¹, (c) 1 s⁻¹, (d) 10 s⁻¹.
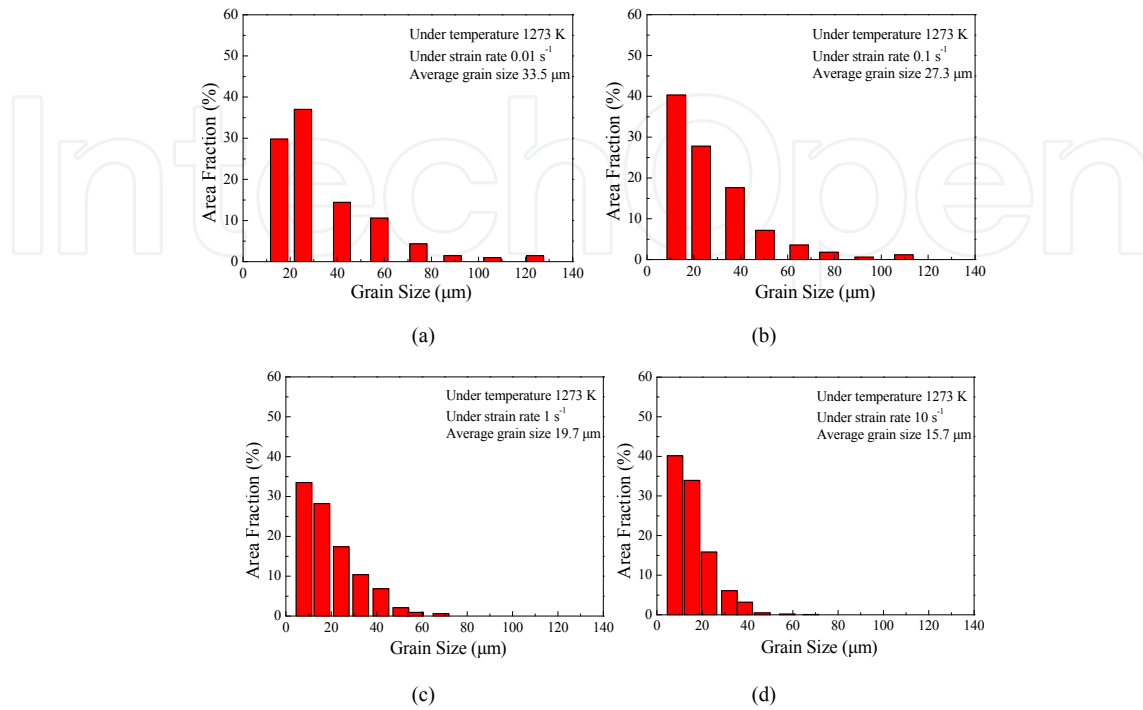

(a)

(b)

(c)

(d)

Figure 21. Grain size distribution of 42CrMo high-strength steel at a fix true strain of 0.9, a fix temperature of 1273 K and different strain rates: (a) 0.01 s⁻¹, (b) 0.1 s⁻¹, (c) 1 s⁻¹, (d) 10 s⁻¹.
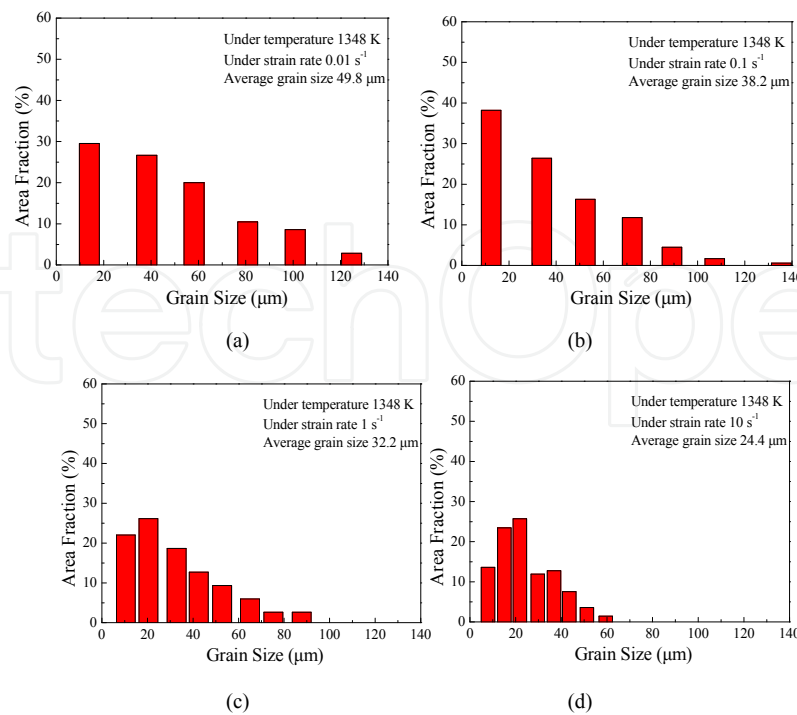
Figure 22. Grain size distribution of 42CrMo high-strength steel at a fix true strain of 0.9, a fix temperature of 1348 K and different strain rates: (a) 0.01 s^{-1}, (b) 0.1 s^{-1}, (c) 1 s^{-1}, (d) 10 s^{-1}.

5. Conclusions

In the deformed material DRX is one of the most important softening mechanisms at high temperatures. DRX occurs during straining of metals at high temperature, characterized by a nucleation rate of low dislocation density grains and a posterior growth rate that can produce a homogeneous grain size when equilibrium is reached. This is a characteristic of low and medium stacking fault energy, SFE, materials e.g., γ-iron, the austenitic stainless steels, and copper. Hot working behavior of alloys is generally reflected on flow curves which are a direct consequence of microstructural changes: the nucleation and growth of new grains, DRX, the generation of dislocations, work hardening, WH, the rearrangement of dislocations, their self-annihilation, and their absorption by grain boundaries, DRV. By the in-depth analysis of the coupling effect in DRX behavior and flow behavior the prediction of DRX evolution can be performed.

The characteristics of softening flow behavior coupling with DRX for as-extruded 42CrMo high-strength steel, as-cast AZ80 magnesium alloy and as-extruded 7075 aluminum alloy have been discussed and summarized as follows: (1) increasing strain rate or decreasing deformation temperature makes the flow stress level increase, in other words, it prevents the occurrence of softening due to DRX and dynamic recovery (DRV) and makes the deformed metals exhibit work hardening (WH); (2) for every curve, after a rapid increase in the stress to a peak value, the flow stress decreases monotonically towards a steady state regime (a

steady state flow as a plateau due to DRX softening is more recognizable at higher temperatures and lower strain rates) with a varying softening rate which typically indicates the onset of DRX, and the stress evolution with strain exhibits three distinct stages; (3) at lower strain rates and higher temperatures, the higher DRX softening rate slows down the rate of work-hardening, and both the peak stress and the onset of steady state flow are therefore shifted to lower strain levels.

Three characteristic points (the critical strain for DRX initiation ($A = 2.44154 \times 10^{25}$), the strain for peak stress ($m = 3.85582$), and the strain for maximum softening rate (ε_c)) which indicate whether the evolution of DRX can be characterized by the process variables need to be identified from the conventional strain hardening rate curves. A modified Avrami equation, ε_p, has been introduced into this work to describe the kinetics of DRX, and then an integrated calculation process has been presented as an example of as-extruded 42CrMo high-strength steel. By the regression analysis for conventional hyperbolic sine equation, the dependence of flow stress on temperature and strain rate was described, and what's more, the activation energy of DRX (ε^*) and a dimensionless parameter controlling the stored energy ($X_{DRX} = 1 - \exp\{-[(\varepsilon - \varepsilon_c)/\varepsilon^*]^m\}$) were determined. In further, the strain for maximum softening rate, Q, and the critical strain, Z/A were described by the functions of ε^*. Thus, the evolution of DRX volume fraction was characterized by the modified Avrami type equation including the above parameters. Based on the calculation results of this model, the effect of deformation temperature, strain and strain rate on the recrystallized volume fraction is as follows: as the strain increases, the DRX volume fraction increases and reaches a constant value of 1 meaning the completion of DRX process; for a specific strain rate, the deformation strain required for the same amount of DRX volume fraction increases with decreasing deformation temperature, which means that DRX is delayed to a longer time; for a fixed temperature, the deformation strain required for the same amount of DRX volume fraction increases with increasing strain rate, which also means that DRX is delayed to a longer time.

The microstructures on the section planes of specimens deformed under different strain rates and temperatures were examined and analyzed under the optical microscope. The evolution of grain boundaries and grain size were presented as an example of as-extruded 42CrMo high-strength steel. It can be summarized that under a fix temperature, as deformation strain rate increases, the microstructure of the as-received billet becomes more and more refined due to increasing migration energy stored in grain boundaries and decreasing grain growth time.

Acknowledgements

Author details

Quan Guo-Zheng

Department of Material Processing & Control Engineering, School of Material Science and
Engineering, Chongqing University, P.R., China

References

[1] Shokuhfar, A, Abbasi, S. M, & Ehsani, N. Dynamic recrystallization under hot defor-
mation of a PH stainless steel. International Journal of ISSI, (2006).

[2] Quan Guo-zhengTong Ying, Luo Gang, Zhou Jie. A characterization for the flow be-
havior of 42CrMo steel. Computational Materials Science, (2010).

[3] Kentaro IharaYasuhiro Miura. Dynamic recrystallization in Al-Mg-Sc alloys. Materi-
als Science and Engineering: A, (2004).

[4] Tsuji, N, Matsubara, Y, & Saito, Y. Dyanamic recrystallization of ferrite in interstitial
free steel. Scripta Materialia, (1997).

[5] Glover, G, & Sellars, C. M. Static recrystallization after hot deformation of α-iron.
Metallurgical Transactions, (1972).

[6] Glover, G, & Sellars, C. M. Recovery and recrystallization during high temperature
deformation of α-Iron. Scripta Materialia, (1973).

[7] Hongyan WuLinxiu Du, Xianghua Liu. Dynamic recrystallization and precipitation
behavior of Mn-Cu-V weathering steel. Journal of Materials Science & Technology,
(2011).

[8] Gourdet, S, & Montheillet, F. A model of continuous dynamic recrystallization. Acta
Materialia, (2003).

[9] Smallman, R. E, & Ngan, A. H. W. Physical Metallurgy and Advanced Materials
(seventh edition), (2007). Elsevier Ltd., Burlington.

[10] Bert VerlindenJulian Driver, Indradev Samajdar, Roger D. Doherty. Thermo-Mechan-
ical Processing of Metallic Materials, Pergamon Materials Series), (2007). Elsevier
Ltd., New York., 11

[11] Guo-Zheng QuanYuan-ping Mao, Gui-sheng Li, Wen-quan Lv, Yang Wang, Jie
Zhou. A characterization for the dynamic recrystallization kinetics of as-extruded
7075 aluminum alloy based on true stress-strain curves. Computational Materials Sci-
ence, (2012).

[12] Guo-Zheng QuanYu Shi, Yi-Xin Wang, Beom-Soo Kang, Tae-Wan Ku, Woo-Jin Song. Constitutive modeling for the dynamic recrystallization evolution of AZ80 magnesium alloy based on stress-strain data. Materials Science and Engineering: A, (2011).

[13] Guo-Zheng QuanTae-Wan Ku, Woo-Jin Song, Beom-Soo Kang. The workability evaluation of wrought AZ80 magnesium alloy in hot compression. Materials & Design, (2011).

[14] Quan Guo-zhengTong Ying, Zhou Jie. Dynamic softening behaviour of AZ80 magnesium alloy during upsetting at different temperatures and strain rates. Proceedings of the Institution of Mechanical Engineers. Part B-Journal of Engineering Manufacture, (2010).

[15] Quan GuozhengLi Guisheng, Chen Tao, Wang Yixin, Zhang Yanwei, Zhou Jie. Dynamic recrystallization kinetics of 42CrMo steel during compression at different temperatures and strain rates. Materials Science and Engineering: A, (2010).

[16] Guo-zheng QuanLei Zhao, Tao Chen, Yang Wang, Yuan-ping Mao, Wen-quan Lv, Jie Zhou. Identification for the optimal working parameters of as-extruded 42CrMo high-strength steel from a large range of strain, strain rate and temperature. Materials Science and Engineering: A, (2012).

[17] Quan Guo-zhengTong Ying, Luo Gang, Zhou Jie. A characterization for the flow behavior of 42CrMo steel. Computational Materials Science, (2010).

[18] Lin, Y. C, & Chen, X. M. A critical review of experimental results and constitutive descriptions for metals and alloys in hot working. Materials & Design, (2011).

[19] Lin, Y. C, Chen, X. M, & Zhong, J. Study of static recrystallization kinetics in a low alloy steel. Computational Materials Science, (2008).

[20] Kim, S. I, & Yoo, Y. C. Dynamic recrystallization behavior of AISI 304 stainless steel. Materials Science and Engineering: A, (2001).